Cancer Nanotechnology

RESEARCH Open Access

Targeting nano-regulator based on metal–organic frameworks for enhanced immunotherapy of bone metastatic prostate cancer

Shu Huang[1], Jun Yuan[1], Yong Xie[1], Kai Qing[1], Zeya Shi[1], Guanyu Chen[1], Jie Gao[1], Haoxiang Tan[1] and Wenhu Zhou[1,2,3*]

*Correspondence:
zhouwenhuyaoji@163.com

[1] Department of Orthopedics, Hunan Provincial People's Hospital (The First-Affiliated Hospital of Hunan Normal University), Changsha 410005, China
[2] Xiangya School of Pharmaceutical Sciences, Central South University, Changsha 410013, Hunan, China
[3] Hunan Provincial Key Laboratory of the Research and Development of Novel Pharmaceutical Preparations, Changsha Medical University, Changsha, China

Abstract

Bone metastasis is the main cause of death in patients with prostate cancer (PCa), but there lacks effective treatment method. Immunotherapy shows new hopes for bone metastatic PCa patients, while the efficacy is still unsatisfactory and limited by the unique immunosuppressive microenvironment in metastatic bone site. Here, we developed a bone-targeted nano-delivery system as a nano-regulator to enhance the immunotherapy of bone metastatic PCa. The nanosystem was assembled via coordination between phytic acid (PA) and Fe^{3+} to form nano-sized metal–organic framework (MOF), through which mitoxantrone (MTO) was encapsulated. At cellular level, the nanosystem showed selective cytotoxicity towards RM-1 PCa cells over immune cells, and could induce tumor cells immunogenic cell death (ICD) to improve the immunogenicity of the tumor. Moreover, the nanosystem was able to induce ubiquitination of TGFβ receptor (TβR) on immune cells to promote its degradation, thus serving as a nano-regulator to block the functions of TGF-β, an abundant cytokine that has a systematically immunosuppressive effect in the tumor microenvironment. Upon intravenous injection, the nanoparticle showed pro-longed blood circulation and targeting accumulation into bone metastatic site, and imposed robust anti-tumor effect in combination with αCTLA-4. In addition, bone destruction was significantly alleviated after treatment to reduce the skeletal-related events. Overall, this work provides a biocompatible nanomedicine to restore immune sensitivity of bone metastatic tumor for enhanced immunotherapy by blocking TGF-β signaling pathway.

Keywords: Nanomedicine, Tumor metastasis, Bone targeting, TGF-β, Mitoxantrone

Introduction

Prostate cancer (PCa) is one of the most common cancers in men, which has a high incidence worldwide. It is a type of inert cancer with high survival rate (up to ~ 100% for 5-year survival), and current available treatments include radical mastectomy and chemical castration (Siegel et al. 2020). However, some patients at advanced cancer

stage undergo metastasis, and such a situation is called metastatic castration-resistant prostate cancer (mCRPC) (Gan et al. 2018). Bone is the most metastatic site of prostate cancer, and the bone metastasis incidence even reaches 90% in mCRPC patients (Gartrell et al. 2015). Once the disease becomes bone metastatic, the 5-year survival rate markedly decreases to 30% (Berish et al. 2018), and the quality of patient life also significantly reduces, accompanied by the occurrence of various skeletal-related events (i.e., severe pain, pathological fractures, spinal cord and nerve compression, and severe pain) (Plunkett et al. 2000; Gao et al. 2021). Surgical treatment is almost impossible for bone metastatic PCa because of several reasons, such as multiple metastatic sites, unclear metastases location, poor physical conditions of the patient, high risk of surgery, as well as recurrence potential. The current palliative therapies such as radiotherapy and chemotherapy, on the other hand, have little effect on overall survival of the patients (Tesfamariam et al. 2019). Therefore, there still remains a challenge to treat bone metastases of mCRPC, and it is highly desirable to explore and develop new methods to meet this clinical demand.

Fortunately, immunotherapy that aims to reinforce the host immune system shows new hope to manage tumor (Farkona et al. 2016). Immunotherapy is a thriving area and has revolutionized the tumor treatment option (Huang and Zhou 2023; Li et al. 2023). Over the past two decades, significant research progress has been made, and several types of immunotherapies, including immune checkpoint therapy (ICT), Chimeric Antigen Receptor T-Cell Therapy (CAR-T), and tumor vaccines, have realized clinical translation to benefit many cancer patients (Feng et al. 2022). Among them, ICT is the most extensively studied subtype, which reverses the immunosuppressive state of tumor by reinforcing the function of T cells (Ding et al. 2022; Zheng et al. 2022). Current, various ICTs have been developed with the targets including programmed cell death protein 1 (PD-1), programmed death ligand 1 (PD-L1) and cytotoxic lymphocyte antigen-4 (CTLA-4), showing encouraging results over a spectrum of tumors and even the metastatic tumors (Li et al. 2020). For instance, the metastatic melanoma patients showed 20–45% response rates with either anti-CTLA-4 or anti-PD-1 therapy (Hodi et al. 2010), whereas the rate can further enhance to 60% upon double checkpoint blockage therapies (Larkin et al. 2015). However, while positive outcome has been observed for a subset of mCRPC patients, the response is still disappointing for those with bone metastases (Sharma et al. 2020). For example, in a phase III clinical trial for the mCRPC patients with ipilimumab (an anti-CTLA-4 ICT), bone metastatic patients showed a worse response than those metastasis of other organs (Beer et al. 2017).

The treatment outcome of immunotherapy highly depends on the tumor microenvironment. Given the poor response of mCRPC bone metastases to ICT, it suggests a different immunological niche in the bone microenvironment as compared to primary tumor and other soft tissue metastases. Actually, metastatic bone site has a unique microenvironment as soil for tumor cell colonization, proliferation, and resistance to immunotherapy. Upon migration into bone tissue, tumor cells release various cytokines to destruct bone by breaking the balance between osteoblasts and osteoclasts (Jiao et al. 2019). Meanwhile, the increased osteoclast activity creates an immunosuppressive microenvironment to promote tumor progression. Recently, a breakthrough finding by Jiao and coworkers showed that transforming growth factor-β (TGF-β) was the

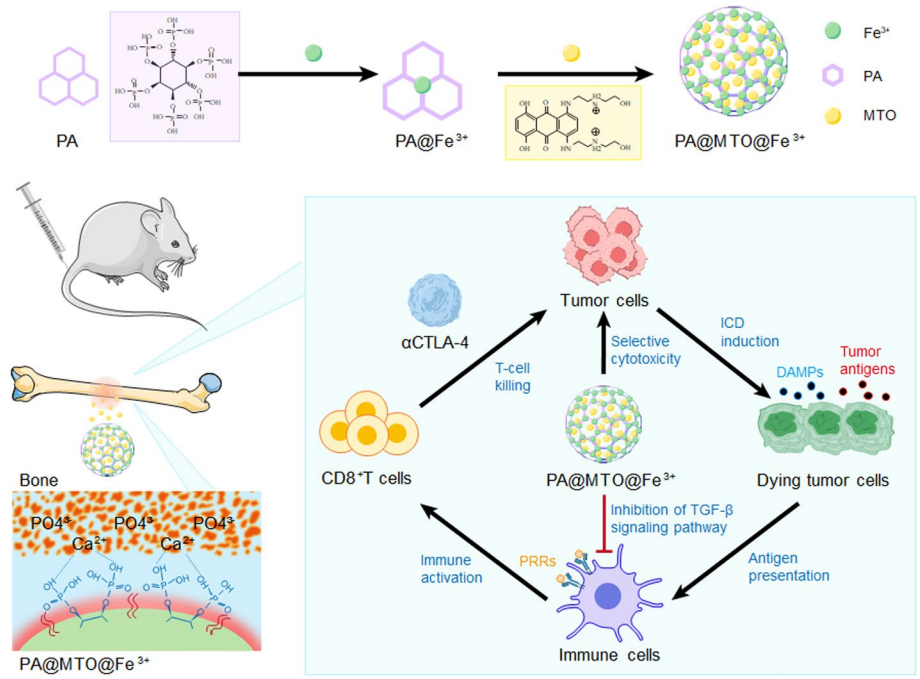

Scheme 1. Schematic illustration of the preparation of MTO@PA/Fe^{3+} MOF and its function mechanisms for targeted immunotherapy of bone metastatic tumor

most important factor in bone metastases to determine immunotherapy resistance (Jiao et al. 2019). TGF-β is an abundant cytokine in bone metastases microenvironment to promote osteoclast differentiation, bone resorption, and destroy the bone. Importantly, TGF-β could promote the polarization of intra-tumoral naive helper T lymphocytes (CD4+ Th cells) into Th17 rather than Th1 lineage, thereby reducing the expression of cytotoxic lymphocytes (CD8+ T cells). Given this fact, TGF-β presents a highly promising target to regulate the therapeutic efficacy of immunotherapy.

In this work, a targeting nano-regulator termed MTO@PA/Fe^{3+} MOF was developed to block the functions of TGF-β for enhanced immunotherapy of bone metastatic PCa (Scheme 1). The nano-regulator was assembled via coordination between Fe^{3+} ion and phytic acid (PA) to form nano-sized metal–organic frameworks (MOFs), with mitoxantrone (MTO) loading into the structure. The MOF structure not only served as a facile payload for drug encapsulation with high loading capacity (30%), but also provided an intrinsic targeting property towards metastatic bone tumors by virtue of enhanced permeability and retention (EPR) effect of tumor and high affinity of PA towards bone tissue (Zhou et al. 2019). Upon targeting delivery, the released MTO as an anti-tumor drug could directly inhibit tumor growth, and induce tumor cells immunogenic cell death (ICD) to promote anti-tumor immunity (Bu et al. 2020). Moreover, MTO bound the receptor of TGF-β on various immune cells surface to induce its degradation, thus abolishing the function of TGF-β. As a result, significantly enhanced anti-tumor effect was achieved in combination with anti-CTLA-4.

Materials and methods

Materials

Mitoxantrone hydrochloride and phytic acid were purchased from Shanghai Yi En Chemical Technology Co., LTD. (Shanghai, China). Phosphate buffer solution (PBS) was purchased from Beijing Dingguo Changsheng Biological Products Co., LTD. (Beijing, China). Rpmi-1640 medium, penicillin–streptomycin mixture, trypsin cell digestion solution and fetal bovine serum were purchased from GIBCO (USA). Anhydrous $FeCl_3$ was from Sigma Aldrich Co., LTD. (Shanghai, China). BCA kit and RIRP lysate were purchased from Beijing Solaibao Technology Co., LTD. (Beijing, China). Dimethyl sulfoxide (DMSO) was purchased from Sinopharm. (Shanghai, China). MTT was purchased from Sigma (USA). Anti-phospho-smad2, Rabbit Anti-Smad2, Rabbit Anti-CRT-FITC and Rabbit Anti-GAPDH were purchased from Beijing Boosen Biotechnology Co., LTD. (Beijing, China). Goat Anti-rabbit IgG-HRP was purchased from Hunan Aijia Biotechnology Co., LTD. (Hunan, China). 4% paraformaldehyde fixation solution was purchased from Suzhou Zeke Biotechnology Co., LTD. (Jiangsu, China). InVivoMab Anti-Mouse CTLA-4 was purchased from BioXcell Co. (USA). Ultrapure water was made in the laboratory.

Cells

Mouse dendritic cells (DC cells), mouse prostate cancer cells (RM-1 cells), and human peripheral leukemia T cells (Jurkat T cells) used in this study were purchased from Shanghai Yuchi Biotechnology Co., LTD. (Shanghai, China). The specific experimental operations were carried out in a sterile ultra-clean workbench. All cells were cultured in RPMI-1640 medium containing 10% FBS, 1% penicillin–streptomycin (50U/mL) in a 5% CO_2 atmosphere at 37 °C.

Animals

Healthy 6-week-old male C57B16j mice were purchased from Hunan SJA Laboratory Animal Co. Ltd. (Changsha, China), and fostered in the SPF Animal experimental center of Hunan Provincial People's Hospital. The daily diet and water activities of mice were not restricted, and the light requirements in line with physiological activities were given. All animal experiments in this study were approved by the Laboratory Animal Ethics Committee of Hunan Provincial People's Hospital and met the requirements of the National Law on the Use of Laboratory Animals of the People's Republic of China.

Preparation and characterization of MTO@PA/Fe^{3+} MOF

At room temperature, 375 μL PA solution (2 mg/mL), 200 μL MTO aqueous solution (0.125 mg/mL) and 750 μL $FeCl_3$ aqueous solution (0.5 mg/mL) were mixed under ultrasonic water bath for 5 min, and then centrifuged (10,000 rpm, 10 min) to remove the supernatant and collect the MTO@PA/Fe^{3+} MOF. The nanoparticles were washed twice by ultrapure water, and resuspended in water at 4 °C for further uses.

The characteristic UV–Vis absorption peak of MTO at 609 nm was used to establish the standard curve for MTO quantification. The MTO content in the supernatant after

centrifugation was quantified to calculate the encapsulation efficiency. The nanoparticles were freeze-dried to obtain the total mass of nanoparticles to allow the quantification of drug loading.

$$\text{Encapsulation efficiency (EE\%)} = \left(1 - \text{MTO content in supernatant/feeding MTO}\right) \times 100\%,$$

$$\text{Drug loading (DL\%)} = (\text{MTO mass in nanoparticles/total mass of nanoparticles}) \times 100\%.$$

The particle size, dispersion coefficient (PDI) and ζ potential of the nanoparticles were measured using a Nano-ZS90 particle size analyzer. The absorption spectrum was detected by uv-2600 uv–visible spectrophotometer. The microstructure of the nanoparticles was studied by Tecnai G2 F20 field emission transmission electron microscope (TEM). The stability of nanoparticles was assessed by redissolving nanoparticles in different buffer conditions (water, PBS, pH 7.4, and 1640 medium containing 10%FBS), and the dynamic size was measured at various timepoints under a 37 ℃ water bath.

In vitro cytotoxicity study

Methyl thiazolyl tetrazolium (MTT) assay was used to test the toxic effect of nanoparticles on cells. The cells were seeded at a density of 5000 cells/well in 96-well plates (100 μL/well), and the periphery of the well plate was blocked with sterile PBS and cultured for 24 h in a cell incubator. The culture substrates were discarded by centrifugation after cell adherence. Then, each formulation with various concentrations was added with 5 multiple Wells in each group. In addition, a cell-free zeroing group and a drug-free control group were set up. The cells were incubated for 24 h, followed by washing twice with PBS. Then, MTT solution (0.5 mg/mL) was added, and the cells were incubated for another 4 h in a cell incubator. After discarding the supernatant, 150 μL DMSO solution was added to each well for 10–15-min incubation at 37 °C in a constant temperature shock chamber. The absorbance value (OD) of each well at 490 nm was measured, and the cell survival rate was calculated.

Induction of immunogenic cell death in vitro

RM-1 cells were seeded in 24-well plates (4×10^4 cells/well) for 24 h incubation, and the culture substrates were discarded. The cells were washed twice with PBS, and free MTO or MTO@PA/Fe^{3+} MOF with equivalent drug concentration of 200 nM was added. A control group without drug was set up. After 4 h incubation, the culturing media and the cells were collected, respectively. The ATP release was calculated by an ATP Assay Kit. For the cell samples, 0.5 μg Anti-CRT-FITC or Anti-HMGB1-FITC antibody was added. The samples were incubated at 4 ℃ for 1 h in the dark, screened, and analyzed by flow cytometry (FCM). Enzyme-linked immunosorbent assay (ELISA) kit was used to detect the expression level of CRT and HMGB1 on RM-1.

Activation and blockade of TGF-β signaling pathway

The expression of P-SMAD protein was detected by Western blot (WB) to detect the expression of TGF-β signaling pathway. DC cells and Jurkat T cells were seeded in 6-well plates (2×10^5 cells/well). Each cell was divided into 4 groups, each with one of the following treatments for 24 h: control group, TGF-β1 group, MTO group, and MTO@PA/

Fe^{3+} MOF group. For free MTO and MTO@PA/Fe^{3+} MOF groups, the equivalent drug concentration was 200 nM. Except for the control group, the other three groups were incubated with TGF-β1 complete medium solution (20 ng/mL) for 30 min. At the end of cell incubation, cells were lysed using RIPA lysate. Then proteins were collected, and the protein concentration was quantified according to the BCA protein quantification method to unify the protein concentration in each group. The resulting protein samples were refrigerated in a −20 °C refrigerator until use. The extracted proteins were detected by gel electrophoresis using Western blot (WB), and finally placed in the visualizer for imaging analysis.

Hemolysis test

The blood was collected and washed with physiological PBS until the supernatant was clarified. The red blood cell suspension was prepared and stored at 4 °C for later use. The blood cell suspension (200 μL) was mixed with nanoparticles (800 μL). The nanoparticles were replaced by pure water for positive control, while the nanoparticles were replaced by normal saline for negative control. After 4 h incubation at 37 ℃, the mixture was centrifuged at 1000 rpm for 5 min. The absorbance value of the supernatant at 577 nm was measured and the hemolysis rate was calculated. Hemolysis rate (%) = (Ab sample − AB negative)/(Ab positive − Ab negative) × 100%.

Pharmacokinetics study

The healthy SD mice were intravenously injected with free MTO or MTO@PA/Fe^{3+} MOF ($n = 4$ for each group, with drug dose of 1 mg/kg). The, the blood samples were collected from the posterior orbital nerve plexus of the mice at each timepoint. The plasma was collected via centrifugation, followed by adding icy methanol to allow protein precipitation. After 90-s vortex, the sample was centrifugated at 12,000 rpm for 15 min. Afterwards, the plasma drug concentration was measured by a HPLC system.

Construction of tumor-bearing tumor model

The right leg of mice was shaved and sterilized. The femoral condyle of mice was drilled with a 1 mL sterile syringe, and then 10 μL of RM-1 cell suspension (1×10^8 cells/mL) was absorbed with a 25 μL micro syringe for cell injection. Four days after tumor cell inoculation, all experimental mice were subcutaneously injected with 100 μL DEGARELIX (50 mg/kg) to establish a castration-resistant prostate cancer bone metastasis model. The tumor formation in the femur of mice was observed regularly. When the tumor grew, the length and width of the tumor were measured with vernier calipers, and the tumor volume was calculated.

Biodistribution study

The tumor-bearing mice were randomly grouped, and administrated with free MTO or MTO@PA/Fe^{3+} MOF with equivalent drug dose of 1 mg/kg. At 12 h after treatment, the mice were killed, and major organs and tumor tissues were collected, weighted and homogenized. After centrifugation, the supernatant was collected for HPLC quantification.

Anti-tumor efficacy evaluation

The tumor-bearing mice were randomly divided into four groups, each receiving one of the following treatments: control; αCTLA-4; MTO@PA/Fe^{3+} MOF; MTO@PA/Fe^{3+} MOF plus αCTLA-4. The drugs were applied at days 0 (when tumors were palpable on the body surface), 3, 6, and 9. The nanoparticles (1 mg/kg MTO) were injected via the tail vein, while CTLA-4 antibody was injected intraperitoneally (the first dose was 8 mg/kg, and the next three doses were 4 mg/kg). Tumor volume was measured every 2 days until the completion of 4 doses, and tumor growth and appearance were recorded. On the 12th day after administration, the whole-body bone CT imaging was performed to observe the bone destruction of the mice in each group. At the same time, the mice were killed to collect the tumors for weighting and pathological analyses.

Safety evaluation

The body weight of mice was measured every other day from the first administration. After treatments, the serum samples were collected to measure the biochemical indexes, and the major organs of the mice were subjected to H&E staining pathological examination.

Statistical analysis

All experimental data were processed by GraphPad-Prism 8.0 software, and statistical analysis was performed by two-sample *t*-test and multi-sample ANOVA comparison. Significance was defined as: $^{*}P < 0.05$, $^{**}P < 0.01$, $^{***}P < 0.001$, and $^{****}P < 0.0001$.

Results and discussion

Preparation and characterizations of MTO@PA/Fe^{3+} MOF

By virtue of abundant phosphate group in its structure, PA could effectively coordinate with Fe^{3+} to assemble into type MOF structure. The coordination ratio of PA/Fe^{3+} was optimized to be 2/1 (w/w) (Additional file 1: Table S1), and the resulting PA/Fe^{3+} MOF displayed a dynamic size ~ 146 nm with PDI of 0.155. We then used such MOF nanoparticles for MTO loading based on our previous reports (Guo et al. 2023; Wang et al. 2022). Interestingly, the feeding MTO concentration has little effect on drug loading efficiency, but affected particle size significantly (Additional file 1: Table S2), and the smallest size of MTO@PA/Fe^{3+} MOF was obtained at 0.125 mg/mL (135 nm, PDI = 0.002) (Fig. 1B). Upon MTO loading, the color of MOF solution changed from light yellow to light blue (Inset in Fig. 1B). From UV–Vis spectra, MTO@PA/Fe^{3+} MOF displayed broad absorbance spectrum from 600 to 700 nm that can be assigned to MTO (Fig. 1C), further demonstrating MTO loading. We then quantified the MTO loading, in which the drug loading and loading efficiency was calculated to be 30% and 85%, respectively. Such high drug loading can be attributable to the strong coordination between MTO and Fe^{3+} to facilitate the drug loading.

The MTO@PA/Fe^{3+} MOF showed a typical MOF morphology with irregular structure (Fig. 1D), and the elemental mapping indicated P, Fe, and N in structure, which were originated from PA, Fe^{3+}, and MTO, respectively. From more detailed TEM

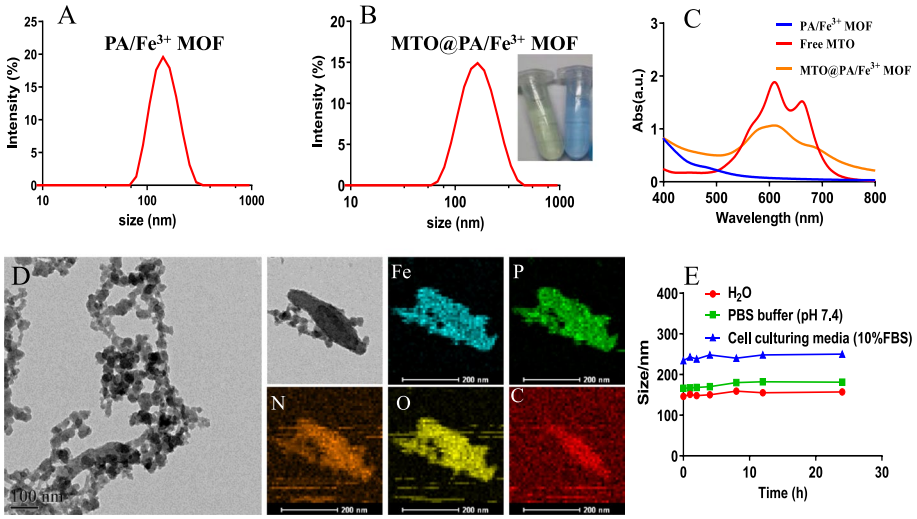

Fig. 1 Hydrodynamic size distribution of **A** PA/Fe^{3+} MOF and **B** MTO@PA/Fe^{3+} MOF. **C** UV–Vis spectra of free MTO, PA/Fe^{3+} MOF, and MTO@PA/Fe^{3+} MOF. **D** TEM images and elemental mapping of the MTO@PA/Fe^{3+} MOF. **E** Colloidal stability of MTO@PA/Fe^{3+} MOF under various conditions

characterization (Additional file 1: Fig. S1), the nanoparticles showed core–shell structures, in which the hydrophobic MTO was loaded into nanocore with the shell layer of PA/Fe^{3+} MOF for stabilization. This result was consistent with our previous work to use MOF for hydrophobic drug loading (Guo et al. 2023; Liu et al. 2020). We also noticed that the particle size observed by TEM was significantly smaller than that of hydrodynamic size, which can be attributable to nanoparticle dehydration before TEM measurement.

The colloidal stability of the nanoparticles was then studied, and the particle size was unchanged over 24 h in both PBS buffer and cell culturing media (Fig. 1E), demonstrating its applicability under biological conditions. Such high colloidal stability can be ascribed to the highly negative charge of the surface with abundant phosphate group (− 33 mV), which provided a strong charge repulsion to inhibit nanoparticles aggregation. Moreover, the negative surface charge could avoid non-specific adsorption of proteins and bio-macromolecules, which also benefits for pro-long stability and circulation in vivo.

Intracellular performances of MTO@PA/Fe^{3+} MOF to damage tumor cells and block TGF-β/SMAD pathway in immune cells

The intracellular performances of the nanoparticles were first studied by measuring cytotoxicity towards tumor cells. Using RM-1 cells prostate cancer cells as example, the anti-tumor activity was tested via MTT assay. A gradual decrease of cell viability was observed over tested concentrations for both free MTO and MTO@PA/Fe^{3+} MOF (Fig. 2A), resulting in IC_{50} value of 34.9 nM and 23.2 nM, respectively. Specifically, MTO@PA/Fe^{3+} MOF achieved slightly higher cytotoxicity than free MTO, likely due to the nanoparticles-mediated delivery to facilitate internalization of the drug. With the capability to damage tumor cells, previous studies have indicated that MTO could also induce tumor cells immunogenic cell death (ICD) to release DAMPs and TAAs (Cheng

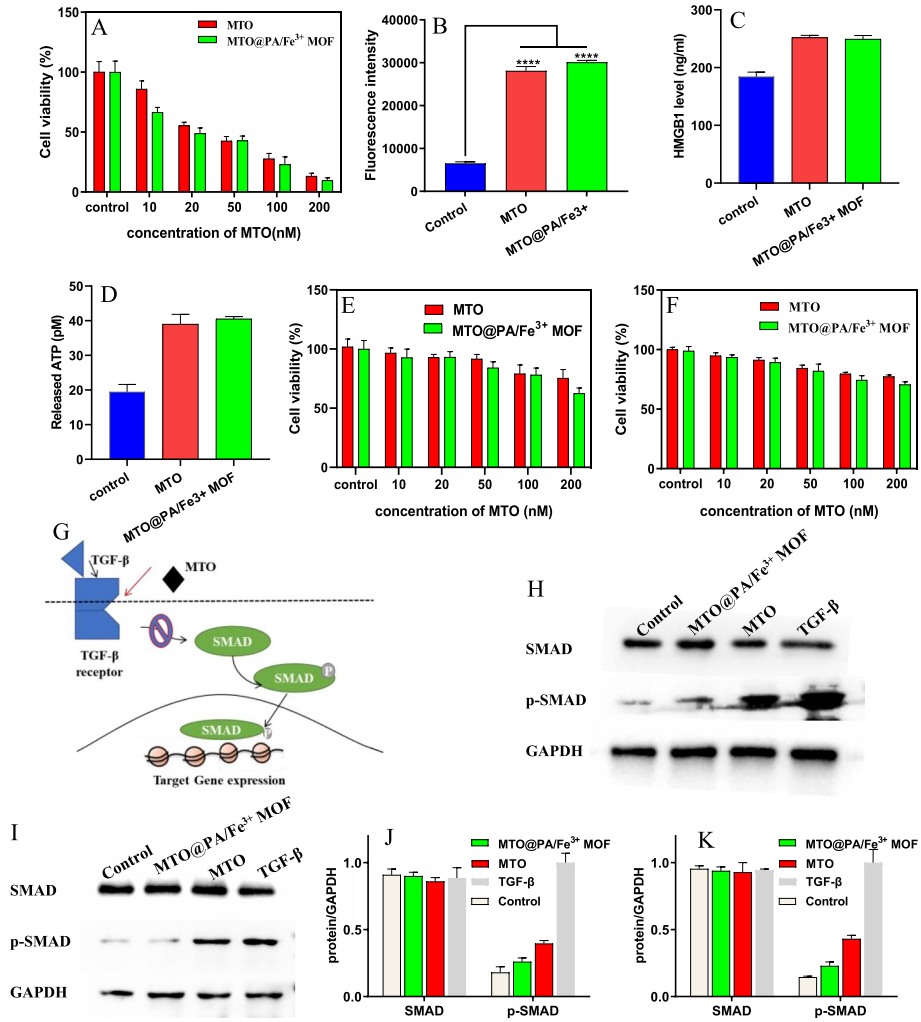

Fig. 2 **A** The cell viability of the RM-1 cells after treatment with free MTO and MTO@PA/Fe^{3+} MOF. **B** CRT exposure, **C** HMGB1 expression, and **D** ATP release for the RM-1 cells treatment with free MTO and MTO@PA/Fe^{3+} MOF. **E** TGF-β/TβR recognition to induce SMAD phosphorylation for signal transduction, and the mechanism of MTO to block TGF-β function. The cell viability of **F** DCs and **G** T cells after treatment with free MTO and MTO@PA/Fe^{3+} MOF. The expression of SMAD and p-SMAD upon various treatments, and the quantified results for **H**, **J** DCs and **I**, **K** T cells

et al. 2020), which benefits to tumor eradication by activating anti-tumor immune responses. To confirm such function, various biomarkers of ICD were measured after treatments, including calreticulin (CRT) exposure, HMGB1 expression, and ATP release. The CRT exposure was studied by flow cytometry, and the intensity was quantified (Fig. 2B), which showed that the signal significantly increased upon treatment with both free MTO and MTO@PA/Fe^{3+} MOF. Likewise, an obvious upregulation of HMGB1 was seen (Fig. 2C), accompanied by the enhanced ATP release (Fig. 2D). The upregulation of CRT could serve as an "eat-me" signal for antigen presenting cells, while the HMGB1 and ATP as s secretory immunostimulant to promote an adaptive immune response. Collectively, MTO@PA/Fe^{3+} MOF not only damaged tumor cells to directly induce an anti-tumor effect, but also induced tumor ICD to trigger an anti-tumor immunity.

Besides directly damaging tumor cells, another important role of MTO@PA/Fe^{3+} MOF is to regulate the function of TGF-β in bone metastatic tissue, which in turn enhanced the efficacy of immunotherapy. Compared to the primary tumor tissue, the bone metastatic tumor is abundant with the cytokine of TGF-β, which has a systematically regulatory effect on various immune cells in the tumor microenvironment, such as DCs and T cells. The recognition of TGF-β by TGFβ receptor (TβR) induces SMAD phosphorylation for signal transduction, which contributes to the suppression of antitumor immunity. It is reported that MTO could increase TβR ubiquitination to promote its degradation, and thus inhibit the function of TGF-β (Jacko et al. 2016) (Fig. 2E). We next studied such activity of MTO@PA/Fe^{3+} MOF. To do this, the cytotoxicity of the nanoparticles to both DCs and Jurkat T cells was evaluated (Fig. 2F, G). Interestingly, compared to tumor cells, both types of immunes cells were more resist to MTO@PA/Fe^{3+} MOF, with most cells still alive even at MTO concentration up to 200 nM. Therefore, MTO@PA/Fe^{3+} MOF had selectivity towards tumor cells over immune cells for tumor therapy without significant side effects.

Next, the blockage effect was evaluated by measuring the SMAD phosphorylation in both DCs and T cells. From the western blot assay, TGF-β treatment could markedly increase the level of p-SMAD (Fig. 2H, I), while the SMAD was not affected, confirming the activation of the signaling pathway. For the cells with co-incubation of free MTO or MTO@PA/Fe^{3+} MOF, by contrast, the p-SMAD remained at low level, demonstrating the suppression effect of the drug on SMAD activation. We further quantified the protein expression, and the consistent results were obtained (Fig. 2J, K). Specifically, MTO@PA/Fe^{3+} MOF displayed relatively better efficacy than free MTO, probably also due to the enhanced drug internalization by nano-delivery system. Therefore, MTO@PA/Fe^{3+} MOF was a robust nano-regulator to block the functions of TGF-β.

Targeting delivery MTO@PA/Fe.$^{3+}$ MOF in bone CRPC model for enhanced efficacy in combination with αCTLA-4

Having confirmed the functions of MTO@PA/Fe^{3+} MOF at cellular level, we next studied its in vivo behaviors. We first studied the in vivo circulation and tumor targetability of the nanoparticles by directly measuring MTO content. The MTO@PA/Fe^{3+} MOF was administrated via intravenous injection, and its hemocompatibility has been confirmed by hemolysis test with less than 5% hemolysis percentage (Fig. 3A, B). The pharmacokinetics were evaluated in health SD rat, and the serum samples were collected for analysis at various timepoints post injection of free MTO or MTO@PA/Fe^{3+} MOF. For free MTO group, the plasma drug concentration sharply decreased from 465 ng/mL to almost background level in 2 h (Fig. 3C), indicating the rapid body clearance of the drug. MTO@PA/Fe^{3+} MOF, on the other hand, showed significantly pro-long in vivo circulation for 12 h, which is beneficial for the decrease of administration frequency with better patient compliance. This long circulation effect can be ascribed the poor kidney filtration of the nanoparticles (Liu et al. 2013). We then studied the biodistribution of the nanosystem in bone CRPC model. To establish the tumor mice model, RM-1 cell suspension was injected into femoral condyle, followed by subcutaneous injection of DEGARELIX at 4 days post inoculation. The major organs were collected for drug quantification, and specific attention was paid

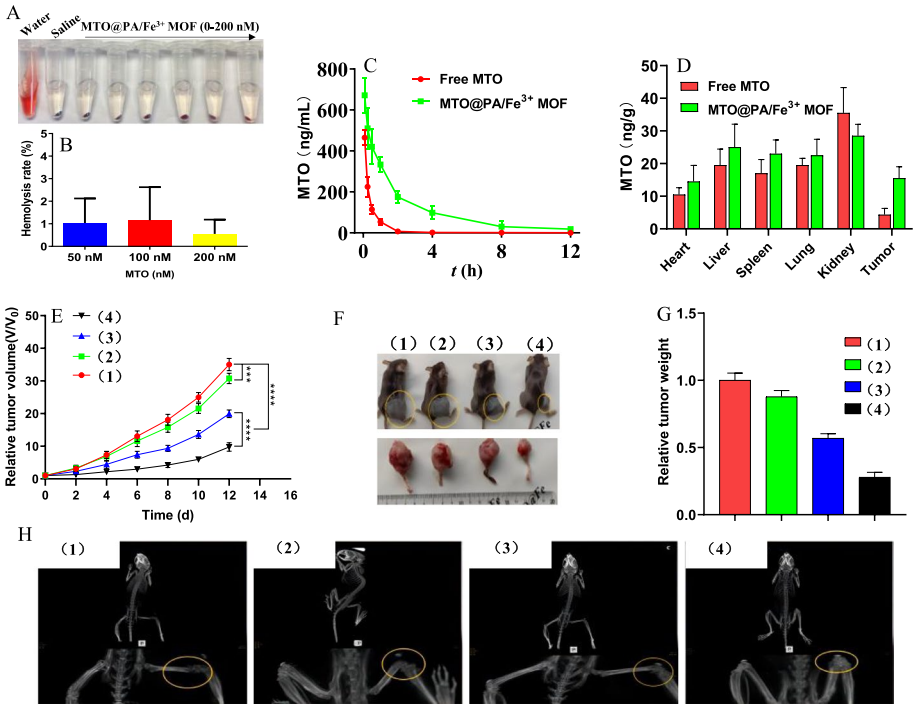

Fig. 3 **A** Hemolysis assay of the nanoparticles at various concentrations. The normal saline and water were employed as negative and positive control, respectively. **B** The quantification of hemolysis rate. **C** The plasm drug concentration–time profile upon intravenous injection of free MTO and MTO@PA/Fe^{3+} MOF. **D** The drug concentration at various tissues at 12 h after intravenous injection of free MTO and MTO@PA/Fe^{3+} MOF. **E** Dynamic monitoring of relative tumor volume after various treatments. **F** The photographs of mice and tumor tissues at day 12 after various treatments. **G** The quantification of relative tumor weight from **F**. **H** The Micro-CT images of mice after various treatments. For each group, (1) control; (2) αCTLA-4; (3) MTO@PA/Fe^{3+} MOF; (4) MTO@PA/Fe^{3+} MOF plus αCTLA-4

on tumor accumulation (Fig. 3D). Notably, MTO@PA/Fe^{3+} MOF achieved more than threefold higher drug concentration than free MTO, confirming the tumor targetability of the nanoparticles. With pro-long circulation, MTO@PA/Fe^{3+} MOF could passively target to tumor via the well-defined EPR effect (Liu et al. 2023). In addition, the surface abundant PA could also facilitate the accumulation of nanoparticles into bone metastatic site by virtue of high affinity between the phosphate groups and bone tissue (Zhou et al. 2019).

Next, the therapeutic efficacy was evaluated, and the model mice were randomly divided into four groups, each receiving the treatment of saline control, MTO@PA/Fe^{3+} MOF, αCTLA-4, and MTO@PA/Fe^{3+} MOF plus αCTLA-4, respectively. For the control group, the tumor grew rapidly with 35-fold volume increase in 12 days. After αCTLA-4 therapy, only marginal tumor growth inhibition was observed, confirming the immunosuppressive microenvironment of the metastatic bone tissue to inhibit the efficacy of immunotherapy. MTO@PA/Fe^{3+} MOF, on the other hand, showed a noticeable anti-tumor effect, which can be ascribed to the tumor damage effect of MTO. Notably, a significant enhanced tumor suppression was achieved for MTO@PA/Fe^{3+} MOF plus αCTLA-4, suggesting an enhanced anti-tumor effect. This can be attributable to TGF-β regulation by MTO@PA/Fe^{3+} MOF to reinforce the activity of

αCTLA-4. The photograph of mice was presented to show the size of tumor tissue at day 12, and the tumor tissue was further collected for direct observation (Fig. 3F). Consistently, the best efficacy was obtained for MTO@PA/Fe^{3+} MOF plus αCTLA-4 based on the tumor weight. In addition, the skeletal-related events of the bone metastasis were also evaluated by the whole-body bone CT imaging (Fig. 3H). For the model group, an obvious bone destruction was observed, while such event was alleviated upon various treatments. Notably, the best efficacy was observed for MTO@PA/Fe^{3+} MOF plus αCTLA-4.

Biosafety evaluation

Finally, the biosafety of the treatments was evaluated. During the treatments, the body weight of all mice did not change (Fig. 4A), indicating the lack of acute toxicity. After treatments, the mice serum was collected, and the representative biochemical indexes were measured, including ALT, AST, BUN and CRE. All these parameters were within the normal range (Fig. 4B, C), suggesting the minimal hepatotoxicity and nephrotoxicity. Moreover, all major organs were collected for H&E staining (Fig. 4D), in which no pathological change was observed for all of the organs. Therefore, the nanomedicine and its combination with αCTLA-4 was highly biocompatible for in vivo applications.

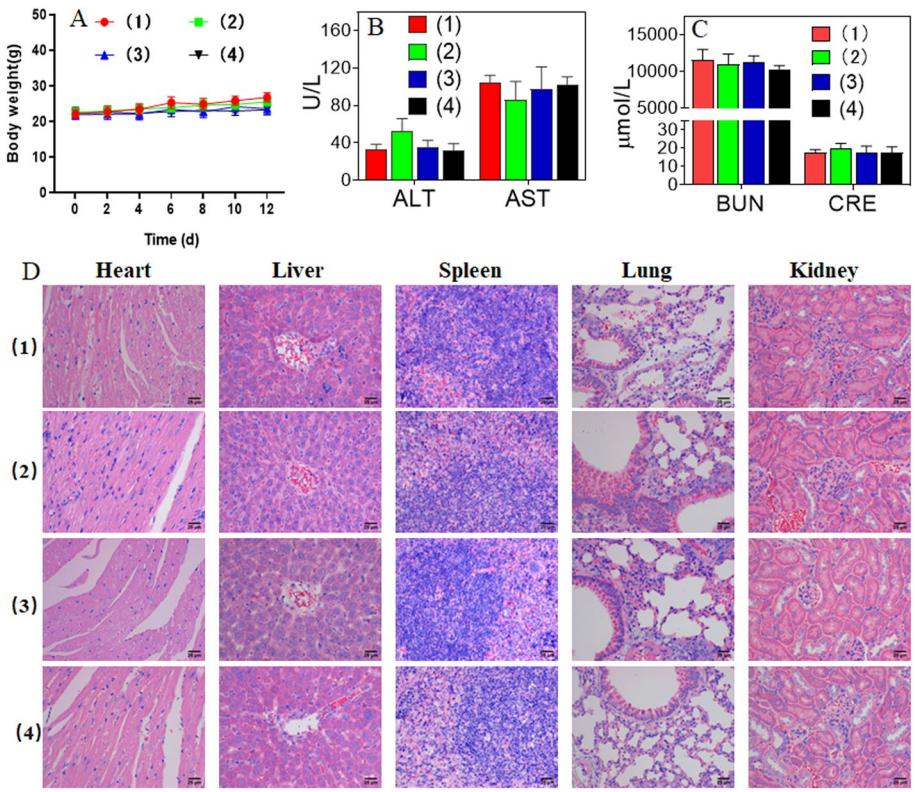

Fig. 4 **A** The dynamic monitoring of body weight of mice during various treatments. **B**, **C** The quantification of various representative biochemical indexes in serum after various treatment. **D** The H&E staining of major organs from mice after different treatments. Scale bar = 25 μm. For each group, (1) control; (2) αCTLA-4; (3) MTO@PA/Fe^{3+} MOF; (4) MTO@PA/Fe^{3+} MOF plus αCTLA-4

Conclusions

In summary, MTO@PA/Fe^{3+} MOF was developed in this work as a nano-regulator to enhance the efficacy of immunotherapy against bone metastatic PCa. The nanosystem was facilely prepared via metal coordination with high drug loading capacity, and its pharmaceutical properties have been systematically characterized. As a nanomedicine, MTO@PA/Fe^{3+} MOF could only not damage tumor cells with high selectivity and induce tumor cells ICD, but also regulate immune cells by blocking TGF-β signaling pathway to enhance the immune sensitivity. The nanomedicine was applied via intravenous injection with high hemocompatibility, which showed significantly pro-longed circulation and enhanced tumor accumulation as compared to the free MTO, demonstrating the advantage of the nano drug delivery system. In bone CRPC model, MTO@PA/Fe^{3+} MOF displayed considerable antitumor effect, and the efficacy was significantly enhanced upon combination of αCTLA-4, demonstrating their enhancement owing to immune regulation activity of MTO@PA/Fe^{3+} MOF. Together with its excellent biocompatibility, such nanomedicine shows great potential for clinical translation to treat bone metastatic tumors.

Supplementary Information

The online version contains supplementary material available at https://doi.org/10.1186/s12645-023-00200-y.

Additional file 1: Table S1. The effect of the weight ratio between PA and $Fe3^{+}$ on the MOF formation (n=3). **Table S2**. Effect of MTO feeding concentration on MTO@PA/$Fe3^{+}$ MOF formation (n=3). **Figure S1**. Detailed TEM characterizations of the MTO@PA/$Fe3^{+}$ MOF.

Acknowledgements
Not applicable.

Author contributions
SH: conceptualization, funding acquisition, investigation, formal analysis, methodology, writing—original draft. JY: investigation, methodology, data analyses, writing—original draft. YX: investigation, formal analysis, methodology. KQ, ZS, GC, JG and HT: investigation, methodology. WZ: conceptualization, funding acquisition, investigation, methodology, supervision, writing—original draft, writing—review and editing. All authors read and approved the final manuscript.

Funding
This work was supported by Hunan Provincial People's Hospital Youth Doctoral Fund Project (BSJJ202220), Foundation of Hunan Provincial Health Commission (C202304078836), and Hunan Provincial Natural Science Foundation of China (2021JJ70016).

Data availability
The raw data and processed data required to reproduce these findings are available from the corresponding author upon request.

Declarations

Ethics approval and consent to participate
All animal experiments in this study were approved by the Laboratory Animal Ethics Committee of Hunan Provincial People's Hospital and met the requirements of the National Law on the Use of Laboratory Animals of the People's Republic of China.

Consent for publication
All authors consent for publication.

Competing interests
The authors declare no competing interests.

Received: 12 March 2023 Accepted: 18 April 2023
Published online: 25 April 2023

References

Beer TM, Kwon ED, Drake CG, Fizazi K, Logothetis C, Gravis G, Ganju V, Polikoff J, Saad F, Humanski P, Piulats JM, Mella PG, Ng SS, Jaeger D, Parnis FX, Franke FA, Puente J, Carvajal R, Sengelov L, McHenry MB, Varma A, van den Eertwegh AJ, Gerritsen W (2017) Randomized, double-blind, phase III trial of ipilimumab versus placebo in asymptomatic or minimally symptomatic patients with metastatic chemotherapy-naive castration-resistant prostate cancer. J. Clin. Oncol. 35:40

Berish RB, Ali AN, Telmer PG, Ronald JA, Leong HS (2018) Translational models of prostate cancer bone metastasis. Nat Rev Urol 15:403–421

Bu YZ, Xu JR, Luo Q, Chen M, Mu LM, Lu WL (2020) A precise nanostructure of folate-overhung mitoxantrone DNA tetrahedron for targeted capture leukemia. Nanomaterials 10:951

Cheng Q, Gao F, Yu WY, Zou MZ, Ding XL, Li MJ, Cheng SX, Zhang XZ (2020) Near-infrared triggered cascade of antitumor immune responses based on the integrated core-shell nanoparticle. Adv Funct Mater 30:2000335

Ding Y, Wang Y, Hu Q (2022) Recent advances in overcoming barriers to cell-based delivery systems for cancer immunotherapy. Exploration 2:20210106

Farkona S, Diamandis EP, Blasutig IM (2016) Cancer immunotherapy: the beginning of the end of cancer? BMC Med 14:73

Feng SJ, Song GX, Liu L, Liu WY, Liang GP, Song ZQ (2022) Allergen-specific immunotherapy induces monocyte-derived dendritic cells but attenuates their maturation and cytokine production in the lesional skin of an atopic dermatitis mouse model. J Dermatol 49:1310–1319

Gan Y, Li LQ, Zhang LW, Yan SJ, Gao C, Hu S, Qiao Y, Tang S, Wang C, Lu ZX (2018) Association between shift work and risk of prostate cancer: a systematic review and meta-analysis of observational studies. Carcinogenesis 39:87–97

Gao YX, Liu YJ, Liu YH, Peng YC, Yuan BW, Fu YX, Qi XL, Zhu QL, Cao TY, Zhang SW, Yin LL, Li X (2021) UHRF1 promotes androgen receptor-regulated CDC6 transcription and anti-androgen receptor drug resistance in prostate cancer through KDM4C-Mediated chromatin modifications. Cancer Lett 520:172–183

Gartrell BA, Coleman R, Efstathiou E, Fizazi K, Logothetis CJ, Smith MR, Sonpavde G, Sartor O, Saad F (2015) Metastatic prostate cancer and the bone: significance and therapeutic options. Eur Urol 68:850–858

Guo J, Liu P, Wei BL, Peng Y, Ding JS, Zhang HL, Zhang GX, Su J, Liu H, Zhou WH, Chen X (2023) Reversing the negative effect of adenosine A1 receptor-targeted immunometabolism modulation on melanoma by a co-delivery nanomedicine for self-activation of anti-PD-L1 DNAzyme. Nano Today 48:101722

Hodi FS, O'Day SJ, McDermott DF, Weber RW, Sosman JA, Haanen JB, Gonzalez R, Robert C, Schadendorf D, Hassel JC, Akerley W, van den Eertwegh AJM, Lutzky J, Lorigan P, Vaubel JM, Linette GP, Hogg D, Ottensmeier CH, Lebbe C, Peschel C, Quirt I, Clark JI, Wolchok JD, Weber JS, Tian J, Yellin MJ, Nichol GM, Hoos A, Urba WJ (2010) Improved survival with ipilimumab in patients with metastatic melanoma. N Engl J Med 363:711–723

Huang A, Zhou W (2023) Mn-based cGAS-STING activation for tumor therapy. Chi J Cancer Res. 35:19–43

Jacko AM, Nan L, Wei J, Zhao J, Zhao Y (2016) Mitoxantrone inhibits TGF beta 1-induced signaling through promoting TGF beta receptor II degradation. J Investig Med 64:962–962

Jiao SP, Subudhi SK, Aparicio A, Ge ZQ, Guan BX, Miura Y, Sharma P (2019) Differences in tumor microenvironment dictate T helper lineage polarization and response to immune checkpoint therapy. Cell 179:1177

Larkin J, Hodi FS, Wolchok JD (2015) Combined nivolumab and ipilimumab or monotherapy in untreated melanoma REPLY. N Engl J Med 373:1270–1271

Li X, Wang L, Chen S, Zhou F, Zhao J, Zhao W, Su C (2020) Adverse impact of bone metastases on clinical outcomes of patients with advanced non-small cell lung cancer treated with immune checkpoint inhibitors. Thoracic Cancer 11:2812–2819

Li LJ, Wang SM, Zhou WH (2023) Balance cell apoptosis and pyroptosis of caspase-3-activating chemotherapy for better antitumor therapy. Cancers (Basel) 15:26

Liu J, Yu M, Zhou C, Zheng J (2013) Renal clearable inorganic nanoparticles: a new frontier of bionanotechnology. Mater Today 16:477–486

Liu P, Liu XJ, Cheng Y, Zhong SH, Shi XY, Wang SF, Liu M, Ding JS, Zhou WH (2020) Core-shell nanosystems for self-activated drug-gene combinations against triple-negative breast cancer. ACS Appl Mater Interfaces 12:53654–53664

Liu R, Luo C, Pang ZQ, Zhang JM, Ruan SB, Wu MY, Wang L, Sun T, Li N, Han L, Shi JJ, Huang YY, Guo WS, Peng SJ, Zhou WH, Gao HL (2023) Advances of nanoparticles as drug delivery systems for disease diagnosis and treatment. Chin Chem Lett. 34:107518

Plunkett TA, Smith P, Rubens RD (2000) Risk of complications from bone metastases in breast cancer: implications for management. Eur J Cancer 36:476–482

Sharma P, Pachynski RK, Narayan V, Flechon A, Gravis G, Galsky MD, Mahammedi H, Patnaik A, Subudhi SK, Ciprotti M, Simsek B, Saci A, Hu YH, Han GC, Fizazi K (2020) Nivolumab plus ipilimumab for metastatic castration-resistant prostate cancer: preliminary analysis of patients in the CheckMate 650 trial. Cancer Cell 38:489

Siegel RL, Miller KD, Jemal A (2020) Cancer statistics, 2020. Cancer J Clin 70:7–30

Tesfamariam Y, Jakob T, Wöckel A, Adams A, Weigl A, Monsef I, Kuhr K, Skoetz N (2019) Adjuvant bisphosphonates or RANK-ligand inhibitors for patients with breast cancer and bone metastases: a systematic review and network meta-analysis. Crit Rev Oncol Hematol. 137:1–8

Wang SM, Liu XJ, Yang MH, Ouyang LQ, Ding JS, Wang SF, Zhou WH (2022) Non-cytotoxic nanoparticles re-educating macrophages achieving both innate and adaptive immune responses for tumor therapy. Asian J Pharm Sci 17:557–570

Zheng Y, Han Y, Sun Q, Li Z (2022) Harnessing anti-tumor and tumor-tropism functions of macrophages via nanotechnology for tumor immunotherapy. Exploration 2:20210166

Zhou ZJ, Fan TQ, Yan Y, Zhang S, Zhou Y, Deng HB, Cai XP, Xiao JR, Song DW, Zhang Q, Cheng YY (2019) One stone with two birds: phytic acid-capped platinum nanoparticles for targeted combination therapy of bone tumors. Biomaterials 194:130–138

Publisher's Note